Halo Profile Engineering to Reduce Vt Fluctuation in High-K/Metal-Gate nMOSFET

W-Y Chen[1,2], T-H Yu[1], Tetsu Ohtou[1], Y-M Sheu[1], Jeff Wu[1], and Cheewee Liu[2]
[1]TCAD Division, Taiwan Semiconductor Manufacturing Company (TSMC)
[2]Department of Electrical Engineering and Graduate Institute of Electronics Engineering, National Taiwan University, ROC
e-mail: wychenv@tsmc.com

***Abstract*—In this work, new halo profile engineering is proposed to suppress the threshold voltage variation (σVt) caused by discrete random dopant fluctuation (RDF). An in-house 3D atomistic numerical simulation tool is utilized to assess nMOSFETs σVt caused by RDF for a HK/MG process. The results show that σVt can be effectively suppressed by 10% by optimizing rotation and tilt angles of the halo implant.**

Keywords-random dopant fluctuation; variability; high-k/metal gate

I. Introduction

With aggressive scaling down of the physical dimensions of CMOSFETs, severe intrinsic process variations become a bottleneck for device/circuit uniformity control. For example, the threshold voltage variation (σVt) is known to be limited by gate length deviation (GLD), line edge roughness (LER) [1], gate electrode work-function (WF) variation [2-5], and discrete random dopant fluctuation (RDF) [6]. RDF is becoming the most dominant factor in σVt for 32nm node and beyond [4]. Optimizing halo profile can be a more feasible and effective way to reduce Vt variation without degrading the saturation current and overlap capacitance, than increasing the doping gradient of the drain-extension profile [7]. In this work, we successfully demonstrate that halo implant profile engineering can effectively suppress nMOSFET σVt by optimizing rotation and tilt angles for a HK/MG process. Co-optimization of halo profile for both performance and σVt is discussed.

II. Transistor Design

The initial simulation templates have been well calibrated with silicon, including junction profiles and electrical characteristics. Subsequently, to achieve the best device performance, ultra shallow junction, spacer dimension, metal gate work function, pocket/LDD, and S/D are further optimized.

III. Modelling of RDF

Figure 1 shows the in-house 3D RDF simulation flow [5]. Starting with a TSUPREM-4 TIF file containing 2D dopant concentration information generated from a well calibrated template, the continuous doping distribution is first converted to distribution of discrete dopants on each grid point, where the number of discrete random dopants is determined by Poisson statistics and the locations of discrete dopants are distributed randomly within the corresponding grid point mech. The resulting discrete dopant distribution is then converted back to the continuous doping profile for further 3D device simulation. The conversion from discrete dopants to continuous dopant distribution is accomplished by taking into account a long-range coulomb potential [8]. The charge density from the long-range part of the ionized coulomb potential for each dopant is computed as shown in (1), to convert the discrete random dopants into the continuous doping profile for further 3D simulation.

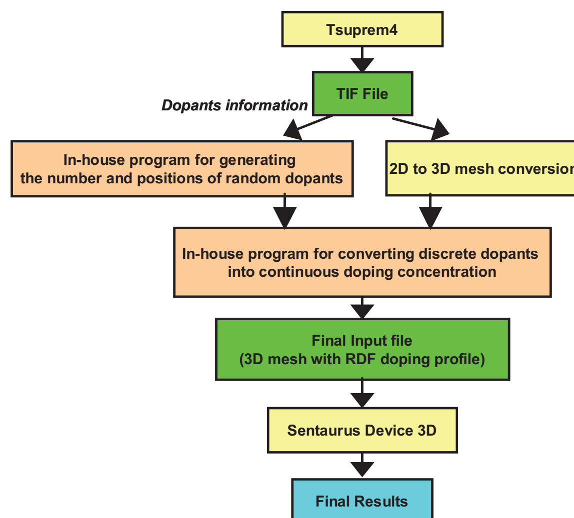

Figure 1 In-house simulation flow for RDF.

$$\rho(r) = \frac{k_c^3}{2\pi^2}\frac{\sin(k_c r) - k_c r\cos(k_c r)}{(k_c r)^3} \quad (1)$$

, where r is the distance to the ionized dopant and k_c is the inverse of the screening length.

The long-range part of the ionized coulomb potential is derived from Fourier transformation of ionized impurity potential in k-space with $|k|<k_c$ as in (2). To keep the total number of discrete dopants conserved, the doping concentration in (1) must be normalized within the device volume in (3) [5]

$$k_c = \sqrt{\frac{q^2 N_A}{\varepsilon k_b T}} \tag{2}$$

, where ε is the dielectric constant and N_A is the acceptor concentration for the p-type substrate.

$$\rho'(r) = \frac{\rho(r)}{\iiint_V \rho(r)dv} = \frac{\rho(r)}{\iiint_V \rho(r) r^2 \sin\theta dr d\theta d\phi} \tag{3}$$

, where V is the device volume, r is the distance to the ionized dopant.

It is well known that fluctuation of dopant location as well as dopant number induces Vt variation [6]. For instance, illustrated in Figure 2, ΔVt (Vt_{RDF}-$Vt_{no\text{-}RDF}$) is 3mV, 27mV, and 46mV, respectively, for three cases with the same total number of channel dopants but different spatial distributions.

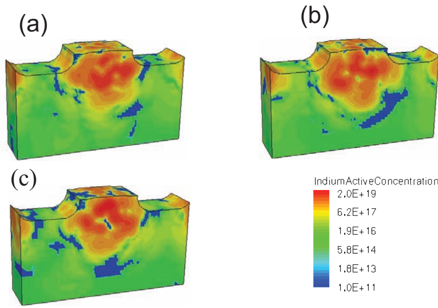

Figure 2 (a),(b), and (c) are 3D halo contours. All cases have same number of channel dopants, but different spatial distributions. ΔVt(Vt_{RDF}-$Vt_{no\text{-}RDF}$) for(a) is 3mV, (b) is 27mV and (c) is 46mV. Only silicon substrate region is shown.

IV. Effect of Halo Rotation on Vt Fluctuation

Three different ways of halo rotation are shown in Figure 3.

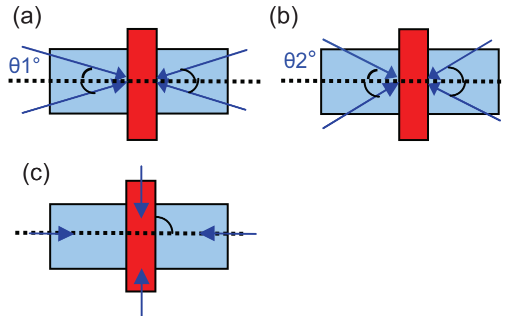

Figure 3 Three different rotation methods for halo implantation: (a) Rθ1, (b) Rθ2and (c) R90.

The rotation angles with respect to channel direction are θ1°, θ2° and 90°, where θ1° < θ2° < 90°, noted herein after as Rθ1, Rθ2 and R90. First, the threshold voltage has been centered so that $Vt_{no\text{-}RDF}$ is the same for all three cases. σVt due to RDF are then simulated and compared in the Pelgrom plots as shown in Figure 4.

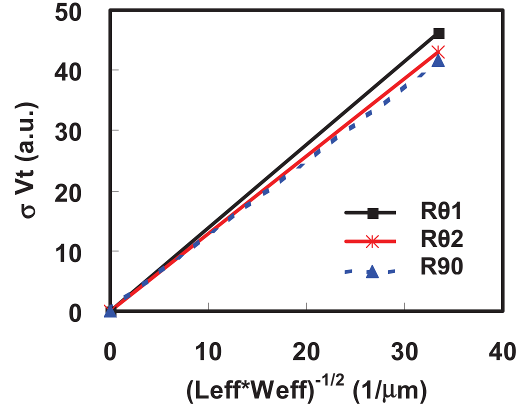

Figure 4 Pelgrom plots of Rθ1, Rθ2 and R90 for HK/MG nMOSFETs. R90 shows 10% σVt reduction compared with Rθ1 due to less confined implant dose under channel region for R90. $Vt_{no\text{-}RDF}$ for Rθ1, Rθ2 and R90 is the same.

R90 shows 10% less Vt fluctuation than that of case Rθ1 and 4% less Vt fluctuation than that of case Rθ2. This can be attributed to the halo dose spreading wider laterally under the gate for case R90 than Rθ1 and Rθ2 as shown in Figure 5, which can reduce Vt sensitivity to dopant profile variation, thus suppress Vt fluctuation. On the other hand, Rθ1 implant causes halo dose more confined near the gate edge than R90 and Rθ2, thus, causing higher Vt sensitivity to dopant profile variations.

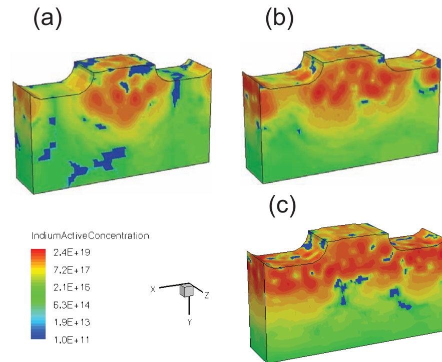

Figure 5 3D halo contour plots for implant rotation (a)Rθ1 ,(b)Rθ2 and (c)R90. Implant dose spreads more under the gate for R90 than with Rθ1 and Rθ2. This larger spread reduces Vt sensitivity to dopant profile variation. Only silicon substrate region is shown. $Vt_{no\text{-}RDF}$ is the same for all cases.

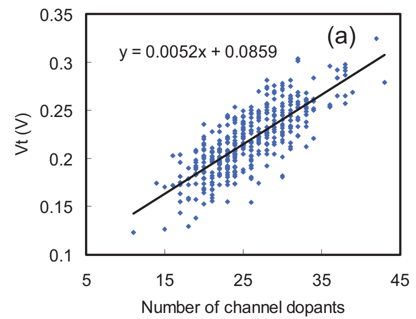

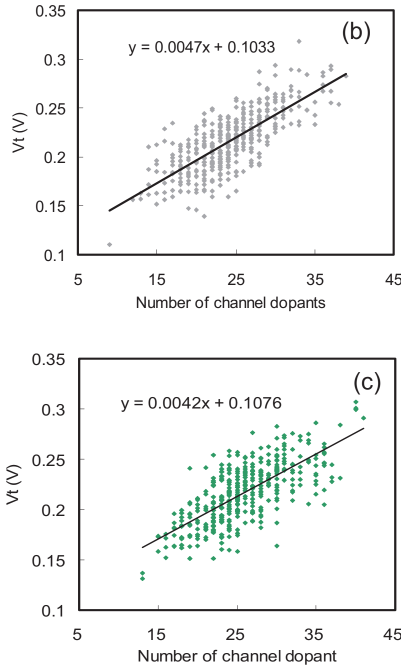

Figure 6 Slope of Vt vs. number of channel dopants. (a) Rθ1 with slope 0.0052 V/(number of channel dopants), (b) Rθ2 with slope 0.0047 V/(number of channel dopants), and (c) R90 with slope 0.0042 V/(number of channel dopants). Smaller slope shows smaller σVt.

As shown in Figure 6, among the three different halo implant rotations, the slope of Vt vs. average number of channel dopants is the smallest for the R90 case. Since the number of channel dopants is comparable in these cases, smaller slope produces smaller Vt fluctuation. Figure 7 shows the normalized short channel control (DIBL) and band-to-band tunneling leakage (Iboff), which are sensitive to junction profiles. When matching Vtsat, Rθ2 shows better DIBL due to better halo confinement, while Rθ1 has smaller Iboff because of less required halo dose. On the other hand, Rθ2 is affected the least by gate height shadowing effect due to implant rotation angle. Therefore, co-optimization of halo rotation angle should be considered.

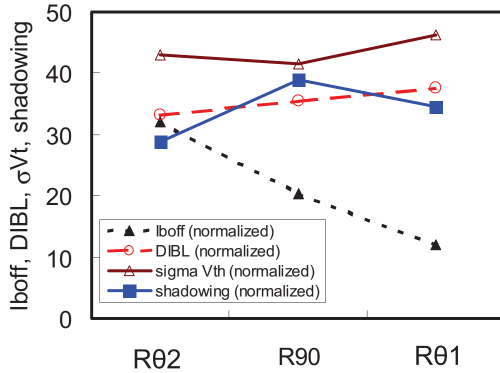

Figure 7 Normalized σVt, Iboff, DIBL and shadowing sensitivity vs. rotation of halo implantation with Rθ1, Rθ2 and R90. $Vt_{no\text{-}RDF}$ is the same for all cases.

V. EFFECT OF HALO TILT ON VT FLUCTUATION

σVt plots for θ2° rotated implant with three tilt angles, T1, T2 and T3 are shown in Figure 8, where T1<T2<T3. Simulations indicate that decreasing halo implant tilt angle can further reduce Vt fluctuation. 3D halo contour plots with the same number of channel dopants, as shown in Figure 9, illustrate that halo dose spreads to a larger area for a smaller halo tilt angle. Vt fluctuation caused by random dopant distribution is reduced for a larger halo dose spreading area.

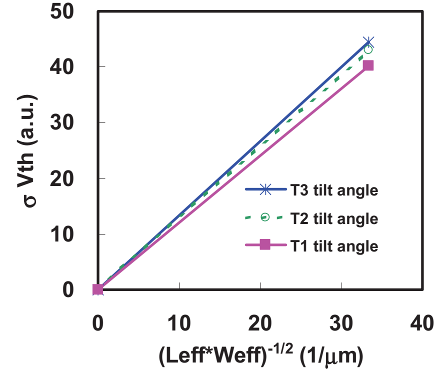

Figure 8 Pelgrom plots of tilt angle T3, T2 , and T1 of HK/MG nMOSFETs. σVt is smallest for tilt T1. $Vt_{no\text{-}RDF}$ is the same T1, T2, and T3.

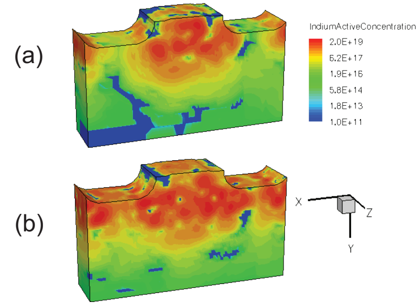

Figure 9 3D halo contour plot for implant tilt angle (a)T3 and (b)T1. Implant dose is less confined under channel region for tilt T1 than T3 which causes smaller σVt for tilt T1. Only silicon substrate region is shown.

Similarly, a smaller halo dose spreading area gives higher Vt sensitivity to dopant distribution, resulting in a larger Vt fluctuation. Furthermore, the channel dopants are more uniformly distributed on the top surface of the channel for the case with T1 tilt implant than that with T3 tilt. This again leads to Vt fluctuation reduction for T1 tilt angle.

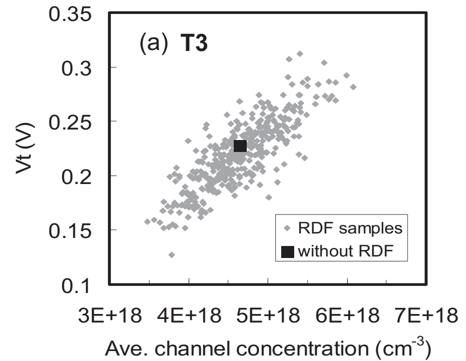

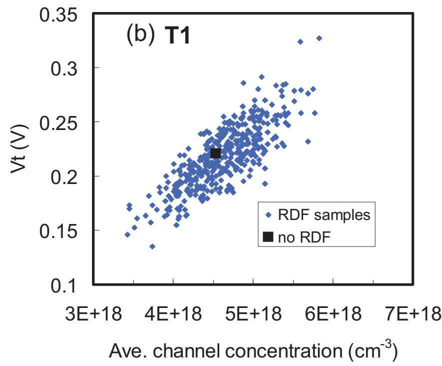

Figure 10 Vt vs. average channel concentration for halo tilt angles (a)T3 and (b)T1. T1 tilt angle case has less scatter than that of T3 tilt angle case and therefore smaller Vt fluctuation.

Figure 10 shows the scatter plot of Vt as a function of average channel concentration. It can be seen that tilt T1 case has smaller scatter cloud thus smaller σVt than that of tilt T3. T1 case shows 10% less Vt fluctuation than that of case T3. It is also observed that the center of the scatter cloud of RDF samples has lower Vt than the non-RDF reference case. This phenomenon is possibly resulted from the higher tendency of dopants to distribute to locations less effective to control Vt than the opposite.

VI. CONCLUSION

We demonstrate that the combination of halo implant rotation and tilt angles can be used to reduce Vt fluctuation in advanced CMOS technology. A 3D atomistic RDF in-house simulator is used to illustrate that a larger halo dose spreading volume leads to a smaller Vt fluctuation. It is also shown that co-optimization of halo profiles is necessary to improve σVt, process control and SCE control.

ACKNOWLEDGMENT

The authors are grateful to Dr. C. H. Diaz for his helpful comments and discussion

REFERENCES

[1] A. Asenov, A. R. Brown, J. H. Davies, S. Kaya, and G. Slavheva, “Simulation of intrinsic parameter fluctuations in decananometer and nanometer-scale MOSFETs,” IEEE Trans. Elec. Dev., p. 1837-1852, 2003.

[2] H. Fukutome, Y. Momoyama, T. Kubo, E. Yoshida, H. Morioka, M. Tajima, and T. Aoyama, “Suppression of poly-gate-induced fluctuations in carrier profiles of sub-50nm MOSFETs,” IEDM Tech, Digest, 2006.

[3] K. Ohmori, T. Matsuki, D. Ishikawa, T. Morooka, T. Aminaka, T. Sugita, T. Chikyow, K. Shiraishi, Y. Nara, and K. Yamada, “Impact of additional factors in threshold voltage variability of metal/high-k gate stacks and its reduction by controlling crystalline structure and grain size in the metal gates,” IEDM Tech, Digest, 2008.

[4] H. Dadgour, K. Endo, V. De, and K. Banerjee, “Modeling and analysis of grain-orientation effects in emerging metal-gate devices and implications for SRAM reliability,” IEDM Tech, Digest, 2008.

[5] T.-H. Yu, T. Ohtou, K.-M. Liu, W.-Y. Chen, Y.-P. Hu, C.-F. Cheng, and Y.-M. Sheu, “Modeling and Optimization of Variability in High-k/Metal-Gate MOSFETs,” SISPAD, 2009.

[6] F.-L. Yang, J.-R. Hwang, H.-M. Chen, J.-J. Shen, S.-M. Yu, Y. Li, and D. D. Tang,” Discrete dopant fluctuated 20nm/15nm-gate planar CMOS,” Symp. VLSI Tech., 2007.

[7] A. Erlebach, T. Feudel, A. Schenk, and C. Zechner, “Influence of HALO and drain-ectension doping gradients on transostor performance,” Mater. Science and Engineering B, pp. 15-19, 2004.

[8] N. Sano, K. Matsuzawa, M. Mukai, and N. Nakayama, “Role of long-range and short-range culomb potentials in threshold characteristics under discrete dopants in sub-0.1um Si-MOSFETs,” IEDM, Tech, Digest, 2000.